FROM OFFSHORE TO ONSHORE PROBABILISTIC TSUNAMI HAZARD ASSESSMENT WITH QUANTIFIED UNCERTAINTY: EFFICIENT MONTE CARLO TECHNIQUES

Gareth Davies[1]

Offshore probabilistic tsunami hazard assessments (PTHAs) are increasingly available for earthquake generated tsunamis. They provide standardized representations of tsunami scenarios, their uncertain occurrence-rates, and models of the deep ocean waveforms. To quantify onshore hazards it is natural to combine this information with a site-specific inundation model, but this is computationally challenging to do accurately, especially if accounting for uncertainties in the offshore PTHA. This study reviews an efficient Monte Carlo method recently proposed to solve this problem. The efficiency comes from preferential sampling of scenarios that are likely important near the site of interest, using a user-defined importance measure derived from the offshore PTHA. The theory of importance sampling enables this to be done without biasing the final results. Techniques are presented to help design and test Monte Carlo schemes for a site of interest (before inundation modelling) and to quantify errors in the final results (after inundation modelling). The methods are illustrated with examples from studies in Tongatapu and Western Australia.

Keywords: tsunami inundation; probabilistic hazard assessment; Monte Carlo methods

BACKGROUND

Probabilistic Tsunami Hazard Assessments (PTHAs) aim to quantify the likelihood of occurrence of tsunamis that meet certain intensity criteria relevant for risk management (Grezio et al., 2017). For instance, a PTHA might estimate the probability of tsunami inundation depths exceeding 1 m in the next 50 years at a particular coastal site. In practice there are large uncertainties in tsunami probabilities that should be accounted for in PTHA, to enable robust risk management decision making (Behrens et al., 2021).

Uncertainties in tsunami probabilities stem from the rarity of hazardous events, and limitations in current-day scientific knowledge of tsunami source processes. Empirical techniques alone cannot accurately quantify the probability of high-consequence tsunamis at most sites, because such events are rare compared to the duration of historical and geological records (Grezio et al., 2017; Behrens et al., 2021). Theory can offer additional constraints, but these are often weak. For example, bounds on maximum earthquake magnitudes are very uncertain for many subduction zones (Berryman et al., 2015); the latter study suggested a maximum magnitude uncertainty range of 8.1-9.6 for the Hikurangi-Kermadec-Tonga subduction zone. Even if the magnitude is fixed, subduction thrust earthquake-tsunamis are affected by other factors (fault geometry, depth, rigidity, and spatial heterogeneity of slip) that cause wave height maxima vary by more than a factor of 10 (Cheung et al., 2022). A key challenge for PTHA is to capture the effect of such 'known unknowns' on tsunami hazards.

For earthquake-generated tsunamis, large-scale 'offshore' PTHAs provide regional databases of hypothetical earthquake-tsunami scenarios, scenario frequency models, and representations of uncertainty in these frequencies (Figure 1). Recent examples include the TSUMAPS/NEAM PTHA in the Mediterranean and northeast Atlantic (Basili et al., 2021) and the 2018 Australian PTHA in the Indian and Pacific Oceans (Davies & Griffin, 2018, 2020). These recent offshore PTHAs represent earthquake-tsunami variability by simulating many stochastic scenarios for each magnitude and source zone, with varying earthquake location, depth and heterogeneous slip. They represent uncertainties in earthquake-tsunami frequencies by considering many alternative scenario-frequency models, each being weighted (e.g. using Bayesian techniques, Figure 1). The aim is to represent tsunami variability, frequency and uncertainty in a manner that can be leveraged for site-specific hazard assessment.

A great benefit of the 'offshore PTHA' approach is that, because tsunamis are modelled for a wide range of sources with a consistent methodology, more data is available for testing. For instance, the 2018 Australian PTHA modelled earthquake-tsunamis on major source-zones in the Indian and Pacific Oceans and used observations from 18 historical tsunamis to statistically test alternative models of tsunami variability (Davies, 2019). Similarly, the earthquake frequency models were tested with paleoseismic data at seven locations in the Indian and Pacific Oceans, as well as spatially aggregated instrumental earthquake observations (Davies & Griffin, 2020). The increased availability of test data at scale gives offshore PTHAs more power to detect and correct methodological biases.

---
[1]Community Safety Group, Geoscience Australia, Cnr Jerrabomberra Ave and Hindmarsh Drive, Symonston, ACT 2609, Australia
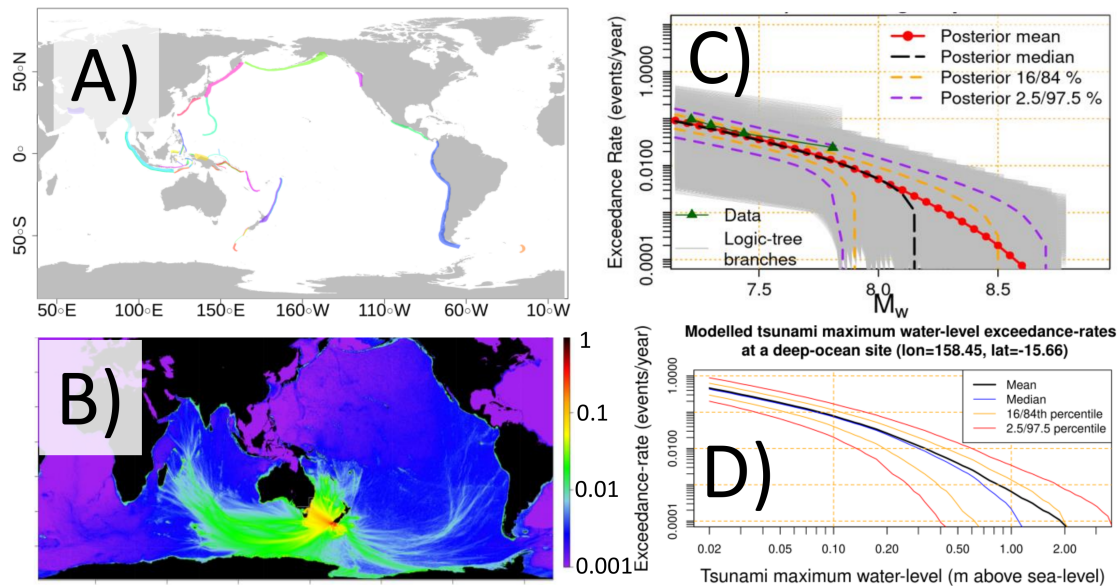
Figure 1: Components of an offshore PTHA (Davies and Griffin, 2018). A) Earthquake source-zones for which tsunami scenarios are modelled. B) An example scenario modelled offshore (1 arcmin grid). The full database contains several hundred thousand such scenarios; C) A magnitude-frequency model for one source-zone (Puysegur, south of New Zealand), with Bayesian credible intervals, used to represent uncertain scenario frequencies; D) Tsunami maxima exceedance-rates at one deep ocean site, with Bayesian credible intervals, derived by combining the scenarios and scenario-frequency models. Similar information is available at thousands of other locations.

The main limitation of offshore PTHAs is that they simulate tsunamis on coarse grids which cannot resolve inundation. Alone, they are insufficient to quantify onshore hazards. But offshore PTHAs can be combined with a site-specific tsunami inundation model to quantify hazards at an onshore site of interest. This is advantageous because inundation hazard studies do not need to derive their own models of scenarios, scenario frequencies and uncertainties. Rather, this information can be extracted from an offshore PTHA which has already been subject to significant testing.

This paper focuses on rigorous yet efficient methods to use offshore PTHAs for site-specific tsunami inundation hazard assessment, while fully representing uncertain tsunami frequencies in the onshore hazard results. The theory is presented more thoroughly elsewhere (Davies et al., 2022); this paper provides a shorter explanation with some new examples. The focus is on earthquake-generated tsunamis, for which offshore PTHAs are most advanced. But the techniques could be applied to other hazards when a large database of coarsely modelled scenarios and frequencies is available, but it is impractical to model all scenarios at high-resolution at the site of interest.

ONSHORE HAZARDS FROM OFFSHORE PTHA
The 'all scenarios' approach

In principle, the best way to translate an offshore PTHA into onshore hazard at a site of interest is to simulate inundation for every scenario $e \in E$, where E is the set of all offshore PTHA scenarios (or some subset of interest, e.g., all scenarios on a particular source zone). The onshore hazard and its uncertainties can then be calculated using the same comprehensive methods used in the offshore PTHA (Figure 1D).

Assume the offshore PTHA represents hazard uncertainties via multiple scenario-frequency models $i \in I$, where I is the set of all alternative scenario-frequency models. For example, grey curves in Figure 1C show alternative scenario-frequency models $i \in I$ for one source-zone (Puysegur) used by Davies & Griffin (2020). These were assigned probabilities ω_i and converted into occurrence-rates for every scenario, with an approach that promotes consistency with earthquake catalogues and spatially variable tectonic convergence rates (details in Davies & Griffin, 2020). For each scenario-frequency model the hazard can be quantified

with exceedance-rate curves λ_i:

$$\lambda_i(Q > Q^T) = \sum_{e \in E} r_i(e)\mathbf{1}_{(Q(e) > Q^T)} \tag{1}$$

Here $\lambda_i(Q > Q^T)$ gives the exceedance-rate (average number of events per year) for which some quantity of interest Q (e.g. maximum depth at a particular site) exceeds a threshold Q^T under scenario-frequency model i. Each scenario e has its own quantity of interest $Q(e)$ determined with high-resolution inundation modelling. The offshore PTHA specifies the long-term occurrence-rate of every scenario e, denoted $r_i(e)$ (events/year), depending on the scenario-frequency model i. The indicator function $\mathbf{1}_{(Q(e) > Q^T)}$ is 1 if $Q(e) > Q^T$, and 0 otherwise. The exceedance-rate uncertainty (i.e. variation with $i \in I$) may be summarised using the mean and percentiles as in Figure 1D (see also Power et al., 2017; Davies & Griffin, 2020; Basili et al., 2021).

The 'all scenarios' approach is common for offshore PTHA, but is rarely practical for onshore hazard assessment because it requires too many inundation simulations. Recent offshore PTHAs include many scenarios, of the order of $10^5 - 10^7$ (Basili et al., 2021; Davies & Griffin, 2018, 2020). In contrast, even when high performance computing is available, recent site-specific studies only model inundation for of the order of $10^2 - 10^4$ scenarios (Tonini et al., 2021; Davies et al., 2022). To support onshore hazard assessment there is a need for alternatives to Equation 1 that do not require inundation modelling for all scenarios.

The 'few scenarios' approach

If few scenarios can be simulated within the computational budget, a common alternative is to select offshore PTHA scenarios with wave heights matching a specified exceedance-rate at some offshore location near the site of interest (e.g. Dall'Osso et al., 2014; Lynett et al., 2016; Kain, 2022; Giblin et al., 2022). This information is readily available in the offshore PTHA (Figure 1D). The modelled inundation for each scenario is then considered to have an exceedance-rate that (approximately) matches that offshore.

This is a pragmatic approach when only few scenarios can be modelled. But it has two significant limitations:

1. Some error is expected in the onshore exceedance-rates, because offshore wave heights are not monotonically related to nearshore and onshore wave heights (Figure 2). For example, even if scenario wave heights match the 1/500 exceedance-rate at the specified offshore site, they will not necessarily have a 1/500 wave height at the coastal site of interest.

2. It is not clear how to estimate the size of this error, while using few scenarios.

The robustness of this approach is improved using multiple scenarios for each exceedance-rate (e.g. Kain, 2022; Giblin et al., 2022). But this increases the computational expense, and it remains unclear how much results would change if using a different set of scenarios, or how well they approximate the 'all scenarios' solution.

The Monte Carlo approach

Monte Carlo methods provide a rigorous alternative, based on modelling inundation for a random subset of offshore PTHA scenarios. Many variations on Monte Carlo methods exist. While generally more computationally expensive than the 'few scenarios' approach, the advantage is that they provably approximate the 'all scenarios' exceedance-rate (Equation 1) while simulating inundation for just a random subset of scenarios (typically far less than the total number of scenarios). The Monte Carlo approximation error varies with the random scenarios, but converges to zero as more scenarios are simulated. Thus the interpretation of Monte Carlo results is clear, and results are repeatable (to within some controllable error) by using a sufficiently large number of random scenarios.

Stratified-sampling by magnitude is to date the most common Monte Carlo approach for inundation PTHA (e.g. De Risi & Goda, 2017; Williamson et al., 2020; Basili et al., 2021; Zamora et al., 2021). As a starting point this splits the set of all scenarios E into multiple bins by magnitude. For example this study uses bins defined by evenly spaced magnitude ranges

$$M_{w,b} \in \left\{(7.15, 7.25], (7.25, 7.35], (7.35, 7.45], \ldots\right\}$$

although uneven ranges could be used. Each magnitude range $M_{w,b}$ has a corresponding bin E_b containing all offshore PTHA scenarios in the magnitude range.
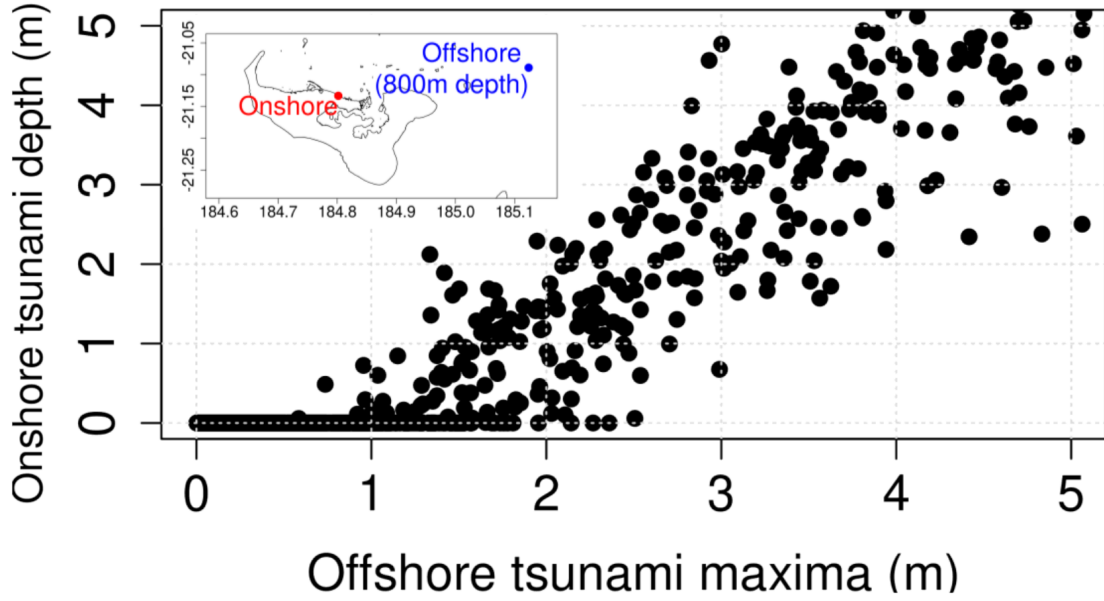
Figure 2: Comparison of offshore tsunami maxima at a deep ocean site (800m depth) and inundation depths at a nearby onshore site (40 km away in Tongatapu, see inset). Points represent approximately one thousand modelled tsunami scenarios on the Kermadec-Tonga trench. Scenarios were selected from the offshore PTHA of Davies and Griffin (2018). For each scenario the tsunami was modelled at high resolution using the earthquake deformation as an initial condition. For details see Davies et al. (2022).

A fixed number $N(M_{w,b})$ of scenarios are randomly sampled from each bin using weighted random sampling with replacement. The $N(M_{w,b})$ values must be determined before sampling, and the Monte Carlo theory herein applies whether the sampling is uniform (i.e. same number in each magnitude bin) or non-uniform (see further discussion in the next section). The sampling weights (i.e. chance of sampling each scenario) are denoted $w_{b,i}^{SS}$ and equal the scenario conditional probabilities defined by the offshore PTHA.

$$w_{b,i}^{SS}(e) = \frac{r_i(e)}{\sum_{e \in E_b} r_i(e)} \quad \text{for scenarios } e \in E_b \tag{2}$$

For each magnitude bin the sampling produces a set of $N(M_{w,b})$ random scenarios, denoted $E_{b,i}^{SS}$.

Inundation is modelled for only these random scenarios. Then the 'all scenarios' exceedance-rate curves may be estimated while only knowing the quantity of interest $Q(e)$ for random scenarios via Equation 3.

$$\widehat{\lambda_i^{SS}}(Q > Q^T) = \sum_{M_{w,b} \in \text{magnitude bins}} \widehat{\lambda_i^{SS}}(Q > Q^T | M_{w,b}) \tag{3}$$

$$\widehat{\lambda_i^{SS}}(Q > Q^T | M_{w,b}) = \lambda_i(M_{w,b}) \widehat{p_{b,i,T}} \tag{4}$$

$$\widehat{p_{b,i,T}} = \left(\sum_{e \in E_{b,i}^{SS}} \mathbf{1}_{(Q(e) > Q^T)} \right) / N(M_{w,b}) \tag{5}$$

$$\lambda_i(M_{w,b}) = \sum_{e \in E_b} r_i(e) \tag{6}$$

Here $\widehat{\lambda_i^{SS}}(Q > Q^T)$ is an *estimate* of the 'all scenarios' exceedance-rate curve defined in Equation 1; the hat notation $\widehat{}$ is used throughout this paper to distinguish Monte Carlo estimates from exact quantities. The key point is that while Equation 3 is approximate, it is much more efficient to compute onshore than the 'all scenarios' solution if the number of random scenarios is not too large.

Note the set of all scenarios E could be restricted to some subset of the PTHA (e.g. a single source-zone), or include multiple sources. If Equation 3 is applied separately to distinct subsets, then results can

later be combined by summation. This is convenient if we know that only a few source-zones affect hazards at the site of interest and prefer to sample each separately.

For illustration Figure 3A shows the variability of tsunami maxima exceedance-rate curves computed with Equation 3; here they approximate the 'all scenarios' solution for the Kermadec-Tonga thrust source in the offshore PTHA of Davies & Griffin (2018). The Monte Carlo solutions broadly follow the 'all scenarios' solution, which is known at this offshore site (Figure 3A). But relative to the correct solution, the spread of the Monte Carlo solutions increases at rare exceedance-rates. In practice this means it can be difficult to accurately represent rare exceedance-rates, which are often of high importance for engineering applications.

EFFICIENT MONTE CARLO SAMPLING ACCOUNTING FOR UNCERTAIN TSUNAMI FREQUENCIES

While Monte Carlo methods can enable rigorous onshore hazard calculations, the error must be controlled to ensure repeatable and accurate results. In practice there is limited capacity to reduce errors by simulating more scenarios, due to the computational expense of inundation models. Thus, it is desirable to have other strategies to reduce errors.

Davies et al. (2022) present an alternative Monte Carlo approach (stratified/importance-sampling) that can reduce errors near a site of interest, by using the offshore PTHA to influence Monte Carlo sampling. Below we give a compact introduction to this approach, which generalises stratified-sampling by magnitude (the latter being a special case). It includes techniques to estimate Monte Carlo errors before inundation computation (to help design robust Monte Carlo schemes) and after inundation computation (to constrain errors in the final inundation hazard results), and strategies that can help to choose the number of scenarios in each magnitude bin $N(M_{w,b})$.

Stratified/importance-sampling

The efficiency of stratified-sampling by magnitude can be improved by leveraging the offshore PTHA tsunami model (available precomputed for every scenario) as an indicator of the scenario inundation potential. For each scenario the user defines a non-negative 'scenario importance' $\mathcal{I}(e)$. For example Davies et al. (2022) used

$$\mathcal{I}(e) = \text{tsunami maxima at an offshore site (near their site of interest)}$$

which is sensible if scenarios with larger offshore wave heights are likely to have larger inundation, all else being equal. We stress that other definitions could also be used, and encourage experimentation with a range of approaches when evaluating schemes prior to sampling (discussed further below). For instance one might try a power-law transformation of the offshore tsunami maxima, or some other transformation that up-weights scenarios with particular wave periods (e.g. when coastal sites of interest are known to be sensitive to particular wave periods). Irrespective, the value of $\mathcal{I}(e)$ should be straightforward to compute for all scenarios.

The chance of sampling each scenario will be scaled by its importance $\mathcal{I}(e)$. This allows better representation of scenarios with high importance, at the expense of less accurately representing scenarios of low importance. Even without a highly accurate scenario importance definition, the approach will converge to the 'all scenarios' solution. However a good scenario importance definition can substantially increase the accuracy for a given sample size (Davies et al., 2022).

As with stratified-sampling, the set of all scenarios E is split into multiple bins E_b corresponding to magnitude ranges $M_{w,b}$. Next a fixed number $N(M_{w,b})$ of scenarios are randomly sampled from each bin using weighted random sampling with replacement. The sampling weights $w_{b,i}^{SIS}$ (i.e. chance of sampling each scenario) are:

$$w_{b,i}^{SIS}(e) = \frac{\mathcal{I}(e)r_*(e)}{\sum_{e \in E_b} \mathcal{I}(e)r_*(e)} \tag{7}$$

where the modeller must choose $r_*(e)$, which should be non-zero for all scenarios that have $r_i(e) > 0$. If only one scenario frequency model $i \in I$ is used, a natural choice is $r_*(e) = r_i(e)$. If in addition $\mathcal{I}(e) = 1$ then the approach reduces to stratified-sampling by magnitude (Equation 2). But more efficient choices can usually be made. Davies et al. (2022) set $\mathcal{I}(e)$ equal to tsunami maxima offshore of their site of interest, while $r_*(e)$ was set equal to the logic-tree mean scenario-frequency model $\bar{r}(e)$. For computational efficiency the latter was used for all scenario-frequency models $i \in I$; this means the sampling weights (Equation 7) do not change and so the same set of random scenarios can be used for calculations involving every alternative scenario-frequency model.
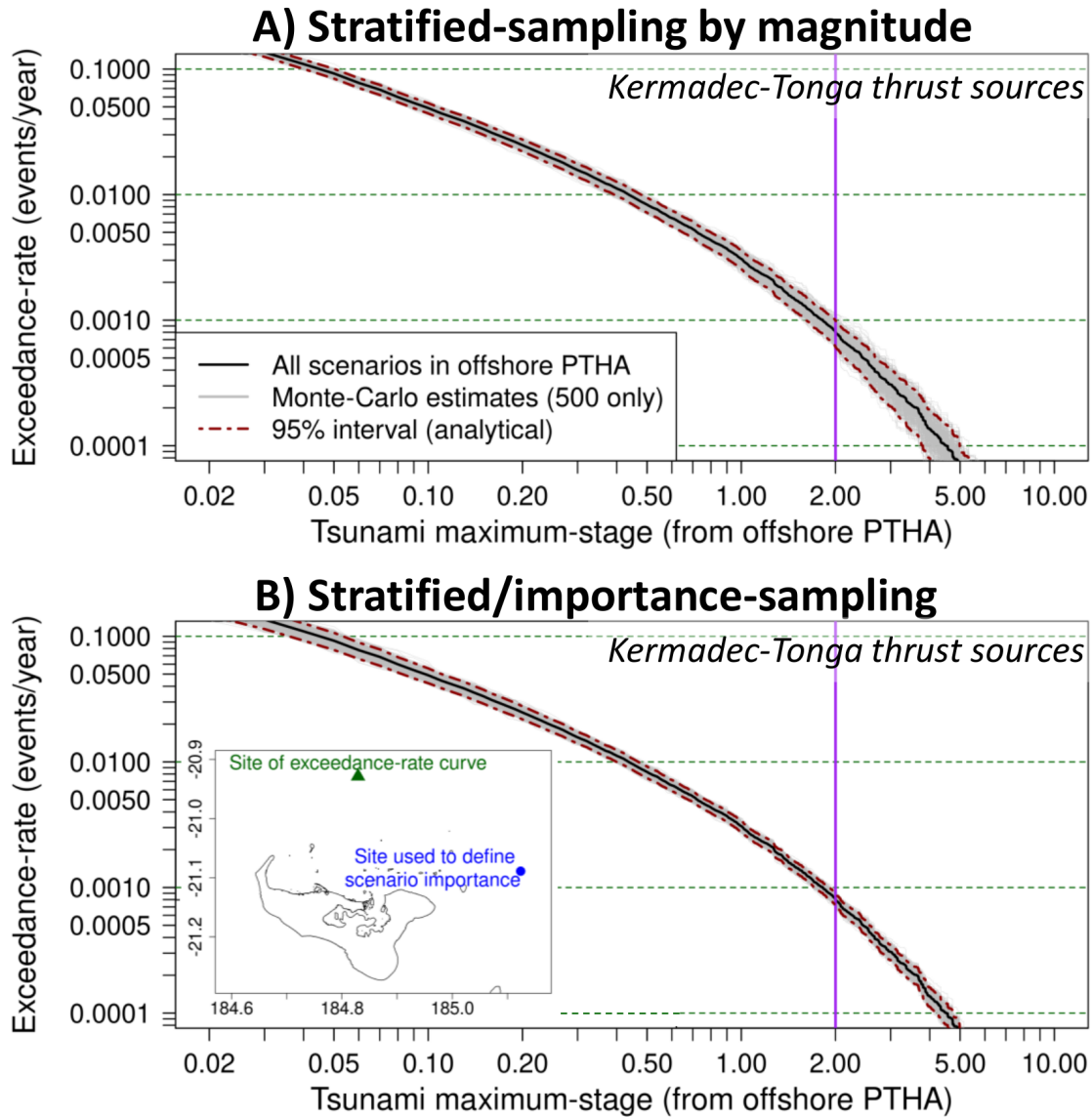
Figure 3: *A)* **Example of stratified-sampling by magnitude at an offshore site north of Tongatapu (location in lower panel inset), adapted from Davies et al. (2022). Black curve shows the logic-tree mean tsunami maxima exceedance-rates for scenarios on the Kermadec-Tonga thrust source zone of an offshore PTHA (Davies & Griffin, 2018). Five-hundred Monte Carlo estimates (grey curves, appearing as a grey region) were derived with Equation 3 using $N(M_{w,b}) = 48$ (1200 scenarios total) and other details matching Davies et al. (2022). The 95% analytical confidence interval was derived using Equation 16.** *B)* **As above using stratified-importance sampling (Equation 8) with non-uniform $N(M_{w,b})$ and the same total number of scenarios as the top panel. The scenario importance $\mathcal{I}(e)$ was equal to the offshore PTHA tsunami maxima at a nearby site (35 km southeast, see inset). Full details in Davies et al. (2022).**

For each magnitude bin the sampling thus produces a set of $N(M_{w,b})$ random scenarios, denoted $E_{b,i}^{SIS}$. Inundation is modelled for only these random scenarios, and the 'all scenarios' exceedance-rate curve (Equation 1) may be estimated via Equation 8:

$$\widehat{\lambda_i^{SIS}}(Q > Q^T) \quad = \sum_{M_{w,b} \in \text{magnitude bins}} \widehat{\lambda_i^{SIS}}(Q > Q^T | M_{w,b}) \tag{8}$$

$$\widehat{\lambda_i^{SIS}}(Q > Q^T | M_{w,b}) \quad = \quad \lambda_i(M_{w,b}) \widehat{q_{b,i,T}} \tag{9}$$

$$\lambda_i(M_{w,b}) \quad = \sum_{e \in E_b} r_i(e) \tag{10}$$

$$\widehat{q_{b,i,T}} \quad = \quad \Big(\sum_{e \in E_{b,i}^{SIS}} \phi_{b,i}^{SIS}(e) \mathbf{1}_{(Q(e) > Q^T)} \Big) / N(M_{w,b}) \tag{11}$$

$$\phi_{b,i}^{SIS}(e) \quad = \quad \Big(\frac{r_i(e)}{\lambda_i(M_{w,b})} \Big) / w_{b,i}^{SIS}(e) \tag{12}$$

This differs from stratified-sampling (Equations 3-6) due to the basic importance-sampling weights $\phi_{b,i}^{SIS}$ which are used to correct for sampling biases. Notice Equations 8-12 reduce to stratified-sampling by magnitude if all $\phi_{b,i}^{SIS}(e) = 1$.

As with stratified-sampling, the method applies whether E is the full set of PTHA scenarios, or some subset (e.g. a particular source-zone). If Equation 8 is applied separately to distinct subsets of scenarios then results may be combined later by summation.

Figure 3B repeats the earlier example using stratified/importance-sampling with the same total number of scenarios and non-uniform $N(M_{w,b})$ as discussed below (full details in Davies et al. (2022)). The scenario importance $\mathcal{I}(e)$ is equal to the offshore PTHA tsunami maxima at a nearby site (35 km southeast). While the same number of inundation calculations are required with this approach, the Monte Carlo errors are much less for large tsunamis (Figure 3). For instance at a threshold $Q^T = 2$ m the Monte Carlo error variance is reduced by a factor of 4.6; it would require 4.6 times more scenarios to make stratified-sampling just as accurate. The accuracy improvements increase for larger tsunamis. This is the key benefit of using the offshore PTHA to inform the Monte Carlo scheme.

Determining typical errors in Monte Carlo exceedance-rates prior to sampling and inundation computation

The exceedance-rate estimate (Equation 8) is unbiased, but will have some error that varies with repeated Monte Carlo sampling. In applications it is desirable to understand the typical size of these errors before finalising the sampling scheme.

To this end, the variance of the Monte Carlo exceedance-rate (denoted $\sigma^2\big(\widehat{\lambda_i^{SIS}}(Q > Q^T)\big)$) can be computed analytically if the quantity of interest $Q(e)$ is known for every offshore PTHA scenario (Davies et al., 2022):

$$\sigma^2\big(\widehat{\lambda_i^{SIS}}(Q > Q^T)\big) \quad = \sum_{M_{w,b} \in \text{magnitude-bins}} \sigma^2\big(\widehat{\lambda_i^{SIS}}(Q > Q^T | M_{w,b})\big) \tag{13}$$

$$\sigma^2\big(\widehat{\lambda_i^{SIS}}(Q > Q^T | M_{w,b})\big) \quad = \quad \frac{\big(\lambda_i(M_{w,b})\big)^2}{N(M_{w,b})} \sum_{e \in E_b} \Big(\big[\mathbf{1}_{(Q(e) > Q^T)} \phi_{b,i}^{SIS}(e) - p_{b,i,T} \big]^2 w_{b,i}^{SIS}(e) \Big) \tag{14}$$

$$p_{b,i,T} \quad = \quad \frac{\sum_{e \in E_b} r_i(e) \mathbf{1}_{(Q(e) > Q^T)}}{\sum_{e \in E_b} r_i(e)} \tag{15}$$

The key point is that if many separate estimates of the Monte Carlo exceedance-rate (Equation 8) were created by repeated sampling, then the variance of the results would converge to Equation 13 as the number of repetitions was increased. Because Equation 8 is unbiased, the variance of the Monte-Carlo exceedance-rates is also the variance of the Monte-Carlo error (the latter having zero mean).

The Monte Carlo exceedance-rate variance (Equation 13) can be computed whether E is the set of all scenarios in the PTHA, or some subset (e.g. a particular source-zone). If results are computed separately for distinct subsets, the variance of their combination can be computed by summing the individual variances.

It is straightforward to compute Equation 13 at offshore sites where the offshore PTHA provides a tsunami model (typically a subset of deep water sites, e.g. Davies & Griffin, 2018). At these sites we can

also compute the 'all scenarios' exceedance-rate (Equation 1), and thus derive an approximate confidence interval for the Monte Carlo exceedance-rates, such as this 95% interval (which assumes a normal distribution):

$$\lambda_i(Q > Q^T) \pm 1.96 \sqrt{\sigma^2\big(\widehat{\lambda_i^{SIS}}(Q > Q^T)\big)} \tag{16}$$

Figure 3 includes 95% confidence intervals derived from Equation 16, highlighting that it can usefully represent the variability of Monte Carlo exceedance-rate estimates.

No random sampling is required to compute this confidence interval (Equation 16). Thus it can be used to estimate the accuracy of a given Monte Carlo scheme offshore, prior to scenario sampling or inundation computation. By constraining the typical Monte Carlo errors (offshore) it is possible to identify poor sampling schemes and experiment with improvements, such as alternative definitions of the scenario importance $\mathcal{I}(e)$, or use of a different number of samples in each magnitude bin $N(M_{w,b})$. While good performance offshore is no guarantee of good performance onshore, in practice it is a useful guide; if the errors are large offshore then it would be surprising to obtain accurate results onshore.

Note Equation 16 provides an approximate confidence interval. It is inexact due to the assumed normality, although that is often a good approximation (Davies et al., 2022). The normal approximation is suggested by theory in special cases. For instance with stratified-sampling ($\phi_{b,i}^{SIS}(e) = 1$) Equation 11 varies like a (scaled) binomial random variable, which is approximately normal with enough samples (e.g. Helsel & Hirsch, 2002; Bolker, 2008). The Monte Carlo exceedance-rate (Equation 8) is a linear combination of such values, so is approximately normal under the same conditions. More generally, even if the distribution is not normal, the Monte Carlo variance (Equation 13) still summarises the expected accuracy of the sampling scheme for any given site, threshold Q^T and scenario-frequency model $i \in I$.

Estimating errors in the final Monte Carlo exceedance-rate after sampling and inundation computation

Once details of the Monte Carlo method are finalised, random scenarios can be sampled and their inundation modelled. Then the modeller will estimate exceedance-rates at sites of interest via Equation 8; these are the key calculations of interest for most applied hazard studies.

To quantify the accuracy of these exceedance-rate estimates, it is useful to have a confidence interval for the 'all scenarios' solution that can be applied at onshore sites, or any other sites where the 'all scenarios' solution is not provided by the offshore PTHA. Equation 17 provides such an approximate 95% confidence interval which is computed using $Q(e)$ values for random scenarios only (Davies et al., 2022):

$$\widehat{\lambda_i^{SIS}}(Q > Q^T) \pm 1.96 \sqrt{\widehat{\sigma^2}\big(\widehat{\lambda_i^{SIS}}(Q > Q^T)\big)} \tag{17}$$

where $\widehat{\sigma^2}\big(\widehat{\lambda_i^{SIS}}(Q > Q^T)\big)$ is an estimate of the Monte Carlo error variance, computed as:

$$\widehat{\sigma^2}\big(\widehat{\lambda_i^{SIS}}(Q > Q^T)\big) \quad = \sum_{M_{w,b}\in\text{magnitude-bins}} \widehat{\sigma^2}\big(\widehat{\lambda_i^{SIS}}(Q > Q^T | M_{w,b})\big) \tag{18}$$

$$\widehat{\sigma^2}\big(\widehat{\lambda_i^{SIS}}(Q > Q^T | M_{w,b})\big) \quad = \frac{\big(\lambda_i(M_{w,b})\big)^2}{N(M_{w,b})} \sum_{e\in E_{b,i}^{SIS}} \Big([\mathbf{1}_{(Q(e)>Q^T)}\phi_{b,i}^{SIS}(e) - \widehat{q}_{b,i,T}]^2/N(M_{w,b})\Big) \tag{19}$$

Equation 17 facilitates estimation of the Monte Carlo error throughout the inundation model domain, including onshore, so is useful for quality control. If Monte Carlo samples are developed separately for multiple distinct subsets of scenarios (e.g. different source-zones), then a confidence interval for their combination can be derived by summing the individual values of $\widehat{\lambda_i^{SIS}}(Q > Q^T)$ and $\widehat{\sigma^2}\big(\widehat{\lambda_i^{SIS}}(Q > Q^T)\big)$ before applying Equation 17.

This confidence interval (Equation 17) is approximate due to the normality assumption and the use of estimates of the mean and variance. The actual coverage probability will vary from case to case but is likely less than 95%. For example Davies et al. (2022) assessed the empirical coverage of Equation 17 under repeated sampling at an offshore site, finding coverage probabilities of 92.65% (stratified-sampling) and 94.55% (stratified/importance-sampling), close to the ideal 95% value. But greater discrepancies are expected for tsunamis that are poorly represented by the sample (very large or very small) so this approximate confidence interval should be interpreted with care.
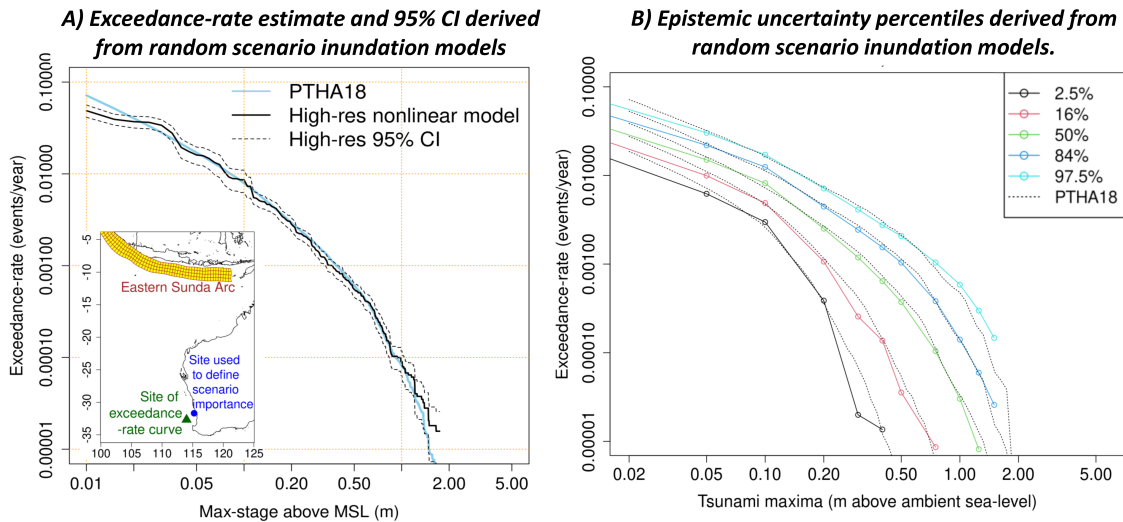
Figure 4: Illustration of stratified/importance-sampling with non-uniform $N(M_{w,b})$ at a site $\simeq 200$ km off-shore of Western Australia (114, -32.666). A set of 390 random scenarios were used to estimate exceedance-rate curves and uncertainties due to earthquake sources (thrust and outer-rise) on the Sunda Arc using an offshore PTHA (Davies & Griffin, 2018, denoted PTHA18). The scenario importance $\mathcal{I}(e)$ was defined as the offshore PTHA modelled tsunami maxima at a nearby site ($\simeq 160$ km northeast), and non-uniform sampling of magnitude bins was applied following Davies et al. (2022). A) Logic-tree mean tsunami maxima exceedance-rate curve, with 95% confidence interval for the all scenarios solution (Equation 17). This agrees well with the 'all scenarios' solution (from the offshore PTHA) which is expected at this offshore site. B) Epistemic uncertainty percentiles which represent uncertain source-frequencies, and comparison with the offshore PTHA solution (denoted PTHA18).

Figure 4A illustrates an 'all scenarios' confidence interval (Equation 17) at a deep water site offshore of Western Australia, which used 390 random scenarios to represent Sunda Arc earthquake sources from the offshore PTHA of Davies & Griffin (2018). For each random scenario the tsunami was modelled from source to inundation with a nonlinear hydrodynamic model (further details below). As the site is deep and well offshore, the confidence interval agrees well with the offshore PTHA's 'all scenarios' solution (Figure 4A), except for the largest and smallest tsunamis that are not well represented by the sample. Greater differences are expected at sites in shallow water or close to the coast due to limitations in the offshore PTHA's linear hydrodynamic model. Although this offshore application provides a useful check on the calculations, in practice the confidence interval is applied at the onshore site of interest, to estimate errors associated with Monte Carlo sampling.

Efficient treatment of epistemic uncertainties

It is desirable to quantify uncertainties in exceedance-rates caused by our lack of knowledge of earthquake source-frequencies. The offshore PTHA represents these epistemic uncertainties with a set of models $i \in I$, each having an associated probability ω_i (Davies & Griffin, 2020). For any site and threshold Q^T this results in a weighted set of exceedance-rates (one per i). Percentiles can be used to summarise the results, e.g., the 84th percentile exceedance-rate is the value such that 84% of the weight is assigned to smaller exceedance-rates.

Epistemic uncertainty calculations thus involve computing exceedance-rates for all scenario-frequency models $i \in I$ (or a large random sample of such models, see Power et al. (2017)). In this situation there is a computational advantage to stratified/importance-sampling (Davies et al., 2022). This is because the within magnitude-bin scenario sampling weights (Equation 7) need not precisely match the scenario conditional probabilities implied by the scenario-frequency model. In contrast, for stratified-sampling they are necessarily the same (Equation 2). If different scenario-frequency models $i \in I$ imply different within magnitude-bin scenario conditional probabilities then, to compute epistemic uncertainties with stratified-sampling, we would have to use different Monte Carlo samples and thus more inundation simulations.

But this is not necessary for stratified/importance-sampling, which can reduce the computational burden of epistemic uncertainty calculations (Davies et al., 2022).

Figure 4B shows epistemic uncertainty percentiles computed with stratified-importance sampling. The site is in deep water offshore of Western Australia, and so we expect results to agree well with the 'all scenarios' solution from the offshore PTHA, as observed (Figure 4B). In practice the same calculations can be applied at onshore sites of interest to quantify epistemic uncertainties.

A subtle issue in epistemic uncertainty calculations concerns dependence in uncertainties on multiple sources-zones, or segments of a single source-zone (Davies & Griffin, 2020; Davies et al., 2022). The calculations herein match the offshore PTHA (Davies & Griffin, 2018) which assumes co-monotonic dependence in uncertainties from different sources. For further details see Davies et al. (2022) who applied the same methods to the Kermadec-Tonga trench.

How many scenarios in each magnitude bin?

The above calculations require choosing the number of scenarios in each magnitude bin $N(M_{w,b})$ prior to sampling and inundation modelling. Typically the total number of scenarios (N_{tot}):

$$N_{tot} = \sum_{M_{w,b}\in\text{magnitude bins}} N(M_{w,b}) \tag{20}$$

is constrained by the computational resources available for inundation modelling. Good choices of $N(M_{w,b})$ will reduce the expected errors in Monte Carlo exceedance rates at the site of interest, while satisfying the constraint on N_{tot}.

For any given N_{tot}, a sampling effort can be determined that minimises the variance of the Monte Carlo errors (Equation 13) given a choice of site, scenario-frequency model i, and threshold Q^T. The solution is (Davies et al., 2022):

$$N_i(M_{w,b}|Q^T) = N_{tot}\sqrt{\alpha_i(M_{w,b}|Q^T)}\Big/\Big(\sum_{M_{w,b}\in\text{magnitude bins}}\sqrt{\alpha_i(M_{w,b}|Q^T)}\Big) \tag{21}$$

$$\alpha_i(M_{w,b}|Q^T) = (\lambda_i(M_{w,b}))^2\Big(\sum_{e\in E_b}([\mathbf{1}_{(Q(e)>Q^T)}\phi^{SIS}_{b,i}(e) - p_{b,i,T}]^2 w^{SIS}_{b,i}(e))\Big) \tag{22}$$

where $N_i(M_{w,b}|Q^T)$ gives the optimal $N(M_{w,b})$ for the chosen site, scenario-frequency model $i \in I$ and threshold Q^T. In practice the $N_i(M_{w,b}|Q^T)$ are rounded to integers.

This optimal solution (Equation 21) can only be computed where the offshore PTHA tsunami model results are stored. Results will vary for other sites, scenario-frequency models and thresholds. But while the solutions are probably not exactly optimal for our onshore sites of interest, they do serve as a guide. For example Davies et al. (2022) selected $N(M_{w,b})$ by combining uniform sampling of magnitude bins (25% of scenarios) with non-uniform sampling (75% of scenarios). The non-uniform sampling was determined by applying Equation 21 offshore of their site of interest using the logic-tree mean scenario-frequency model, and averaging the solutions for a range of thresholds. To confirm that efficiency improvements were expected the results were checked by studying the performance at other nearby offshore PTHA sites, before final sampling and inundation modelling.

A similar approach was implemented for the Western Australian calculations shown previously (Figure 4). Scenarios were sampled separately for the dominant Sunda Arc thrust source ($N_{tot} = 320$) and the secondary Sunda Arc outer-rise source ($N_{tot} = 70$). For each case the optimal sampling effort was computed with thresholds $Q^T = 1, 2$ via Equation 21, using the logic-tree mean scenario-frequency model offshore the site of interest. Figure 5 shows results for Sunda Arc thrust scenarios; this highlights that greater thresholds tend to concentrate samples in large magnitude bins. The final $N(M_{w,b})$ was chosen as a 25%:75% combination of the uniform and average non-uniform solutions.

By using 25% uniform sampling the approach gains robustness in situations where Equation 21 is far from optimal. This may be relevant for atypical scenario-frequency models (very different to the logic-tree mean model) which can influence epistemic uncertainty calculations. The use of non-uniform sampling for the remaining 75% of scenarios is expected to improve the accuracy for more typical scenario-frequency models. In practice the choice of $N(M_{w,b})$ should be checked at a range of sites before sampling and inundation modelling, using techniques discussed above.
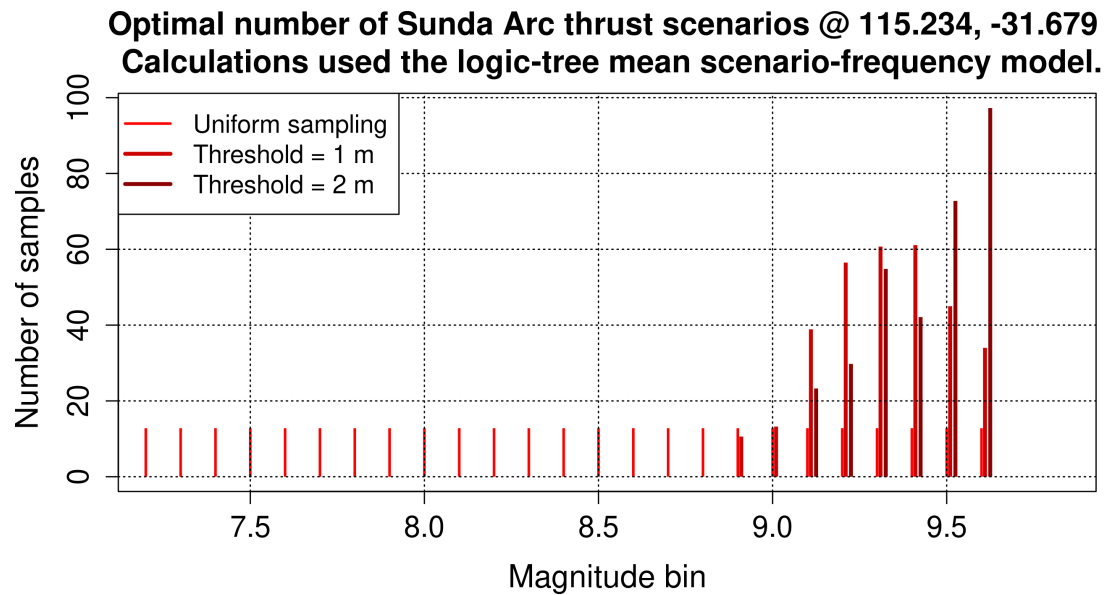
Figure 5: Optimal number of Sunda Arc thrust scenarios per magnitude-bin at site offshore of Western Australia (as used to define the scenario importance in Figure 4). Calculations assume N_{tot} = 320 and use the logic-tree mean scenario-frequency model from Davies & Griffin (2018). Results vary depending on the threshold Q^T.

ESTIMATING RATES OF TSUNAMI INUNDATION IN SW WESTERN AUSTRALIA, DUE TO SUNDA ARC EARTHQUAKES

Stratified/importance sampling was applied for tsunami inundation hazard modelling near Perth in Western Australia, considering only earthquakes on the Sunda Arc (Figure 6). Random scenarios from the offshore PTHA of Davies & Griffin (2018) were simulated from earthquake source to inundation with the model SWALS, which solves the shallow water equations on two-way nested grids in spherical or Cartesian coordinates (Figure 6). Tsunami propagation in the broader Indian Ocean was represented at relatively coarse resolution (1 arcmin cells) with the linear shallow water equations plus an additional nonlinear Manning friction term; these equations were solved with a leapfrog scheme (Davies et al., 2020). A series of two-way nested grids (grid cells of 1/9, 1/54 and 1/162 arcmin) were used achieve $\simeq$ 10 m resolution in the Greater Perth region; on these grids the full nonlinear shallow water equations with Manning friction were solved via a second order accurate finite-volume scheme (Davies et al., 2020). Each tsunami was simulated for 24 hours and required $\simeq$ 2.7 hours of computation per scenario using 6 nodes (288 cores) of the Gadi supercomputer.

The model was tested by simulating 2 historic Sunda-Arc tsunamis (2004/12/26 Sumatra M_w9.2 and 2005/03/28 M_w8.6), both well observed on tide-gauges in the Greater Perth region. Every modelled scenario was checked to confirm mass conservation and energy decay, and convergence tested by comparison with an identical simulation on a 2x coarser grid. The SWALS code has been used to model many tsunamis both in the deep ocean and nearshore (Davies & Griffin, 2018; Davies, 2019; Davies et al., 2020, 2022) and is distributed[2] with 27 analytical, experimental and field test programs that include well-known tsunami benchmarks (non-landslide problems in NTHMP (2012), and all problems in NTHMP (2017)).

Two deliberately conservative choices were made in the inundation model setup:

1. All simulations employ a constant background sea-level of +0.6m AHD, close to the highest astronomical tide at the site of interest (AHO, 2022).

2. A constant Manning friction value was used (n = 0.03) which is likely too low in areas with heavy vegetation or buildings.

---

[2]https://github.com/GeoscienceAustralia/ptha/tree/master/propagation/SWALS
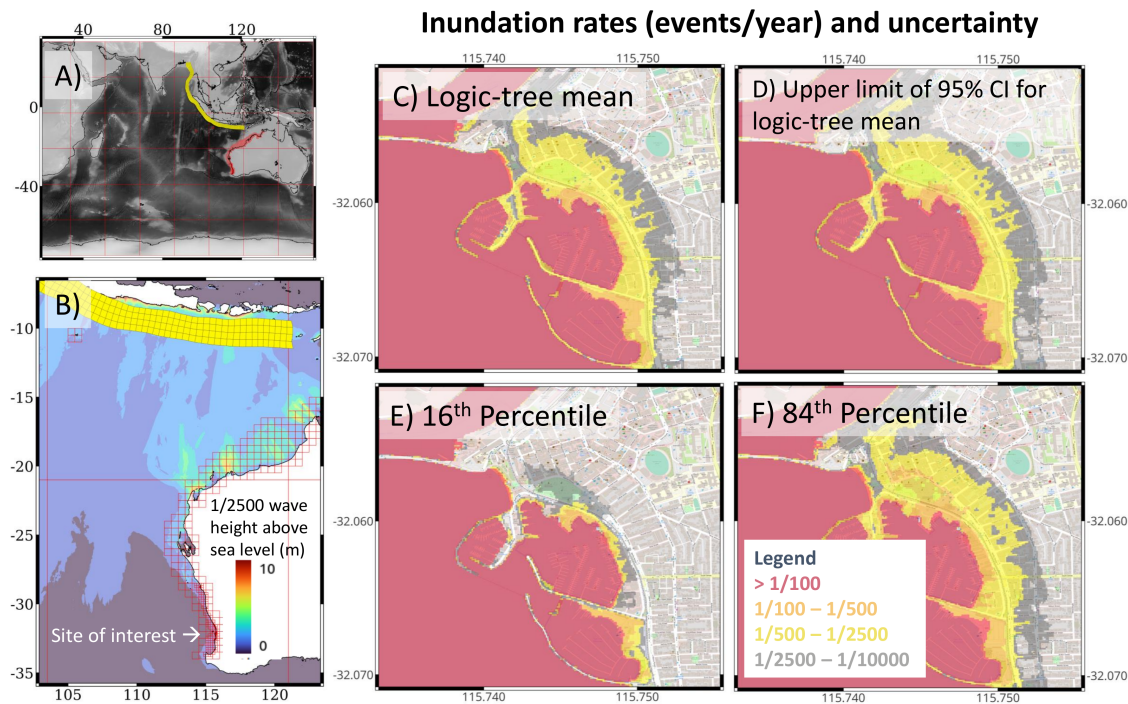
Figure 6: Example of inundation hazard calculations in SW Western Australia derived with strati-fied/importance sampling. *A)* **Model domain with Sunda Arc source (yellow) and hydrodynamic model nested grids (red).** *B)* **Location of site of interest. Background shows tsunami maxima above sea level having a 1/2500 exceedance-rate (logic-tree mean) computed with stratified/importance sampling.** *C-F)* **Modelled rate of inundation (depth > 1 mm) and uncertainties in a small part of the model, assuming a conservative background sea-level (0.6 m above mean sea level) and constant friction ($n = 0.03$). Results show the logic-tree-mean (C), upper limit of a 95% confidence interval for the logic tree mean using Equa-tion 17 (D), 16th percentile epistemic uncertainty (E) and 84th percentile epistemic uncertainty (F).**

This implies the modelled inundation exceedance-rates are conservative, which fits our end-user needs. Treatment of dynamic tides would complicate the modelling but should be considered in future work.

Stratified/importance sampling was applied separately to the thrust and outer-rise Sunda-Arc sources in the offshore PTHA (Davies & Griffin, 2018). Based on preliminary model run times and available computational resources, the total number of scenarios was set to 390. The offshore PTHA suggested thrust sources would be most significant, so we sampled more thrust scenarios (N_{tot} = 320) than outer-rise scenarios (N_{tot} = 70). In both cases the scenario importance $\mathcal{I}(e)$ was set equal to the offshore PTHA tsunami maxima at a site offshore of Perth (lon=115.234, lat=-31.679). The sampling effort in each magnitude bin $N(M_{w,b})$ was set as described earlier. Preliminary estimates of Monte Carlo errors offshore (using techniques similar to Figure 3) suggested the accuracy would be sufficient for our needs. Following inundation modelling we confirmed that the Monte Carlo results were quite consistent with the offshore PTHA in deep water (Figure 4).

Figure 6C-F depicts inundation exceedance-rates in a small part of the model, which are conservative for reasons discussed above. The logic-tree mean result (Figure 6C) shows only minor inundation at exceedance-rates greater than 1/500, but the inundation zone grows for rarer events. To check the accuracy of this result, Figure 6D shows the upper limit of a 95% confidence interval for the 'all scenarios' solution (Equation 17). This is similar to the logic-tree mean result (Figure 6C) suggesting that errors due to Monte Carlo sampling are small.

The modelled inundation frequencies are strongly affected by epistemic uncertainties in earthquake frequencies (Figure 6E-F). The 16th percentile result shows relatively minor inundation. The 84th percentile results are similar to the logic-tree mean but with a more extensive inundation at exceedance-rates > 1/500. The difference in these results is significant and shows that weak constraints on large earthquake frequencies lead to substantial uncertainties in the chance of inundation. This makes sense considering that earthquakes on the eastern Sunda Arc are best placed to affect the site. While the large fault area and rapid tectonic convergence of the eastern Sunda Arc suggests the potential for large earthquakes (McCaffrey, 2009; Berryman et al., 2015), the largest historical earthquake (M_w8.3) is small compared with the 2004 Sumatra-Andaman earthquake (M_w9.2) which occurred further west. This increases the uncertainty of large earthquake frequencies in the east, as represented by the offshore PTHA (Davies & Griffin, 2018). A key advantage of probabilistic tsunami hazard assessment is that these uncertainties can be quantified and communicated to decision makers, who can make risk trade-offs appropriate to their particular problem.

CONCLUSION

Monte Carlo methods are attractive for transforming offshore PTHAs into onshore hazard information. They can rigorously approximate the 'all scenarios' solution while simulating inundation for just a fraction of scenarios and retaining information on epistemic uncertainties. Stratified/importance-sampling enables more computational effort to be spent on scenarios that are important at the site of interest, without introducing statistical biases (Davies et al., 2022). The resulting Monte Carlo errors are well understood theoretically. This facilitates testing and improving the sampling scheme prior to inundation computation, and the estimation of errors in the final results. The approach is useful at both near-field and far-field sites (i.e. near or far from the earthquake source).

Future work should further investigate strategies to account for multiple source-zones. In this study the Sunda Arc thrust and outer-rise sources were treated separately, and while this gives the modeller substantial control, in cases with many source-zones it may be more efficient to sample directly from a combined source. There is also a need to account for the effect of dynamic tides, for example by including the tidal phase in the scenario importance measure. This would likely reduce the modelled inundation exceedance-rates.

References
AHO, 2022. Australian national tide tables 2022, Tech. rep., Australian Hydrographic Office.

Basili, R., Brizuela, B., Herrero, A., Iqbal, S., Lorito, S., Maesano, F. E., Murphy, S., Perfetti, P., Romano, F., Scala, A., Selva, J., Taroni, M., Tiberti, M. M., Thio, H. K., Tonini, R., Volpe, M., Glimsdal, S., Harbitz, C. B., Løvholt, F., Baptista, M. A., Carrilho, F., Matias, L. M., Omira, R., Babeyko, A., Hoechner, A., Gurbuz, M., Pekcan, O., Yalciner, A., Canals, M., Lastras, G., Agalos, A., Papadopoulos, G., Triantafyllou, I., Benchekroun, S., Agrebi Jaouadi, H., Ben Abdallah, S., Bouallegue, A., Hamdi, H., Oueslati, F., Amato, A., Armigliato, A., Behrens, J., Davies, G., Di Bucci, D., Dolce, M., Geist, E., Gonzalez Vida, J. M., Gonzalez, M., Macias Sanchez, J., Meletti, C., Ozer Sozdinler, C., Pagani, M., Parsons, T., Polet, J., Power, W., Sørensen, M., & Zaytsev, A., 2021. The Making of the NEAM Tsunami Hazard Model 2018 (NEAMTHM18), *Frontiers in Earth Science*, **8**.

Behrens, J., Løvholt, F., Jalayer, F., Lorito, S., Salgado-Galvez, M. A., Sørensen, M., Abadie, S., Aguirre-Ayerbe, I., Aniel-Quiroga, I., Babeyko, A., Baiguera, M., Basili, R., Belliazzi, S., Grezio, A., Johnson, K., Murphy, S., Paris, R., Rafliana, I., De Risi, R., Rossetto, T., Selva, J., Taroni, M., Del Zoppo, M., Armigliato, A., Bures, V., Cech, P., Cecioni, C., Christodoulides, P., Davies, G., Dias, F., Bayraktar, H. B., Gonzalez, M., Gritsevich, M., Guillas, S., Harbitz, C. B., Kanoglu, U., MacÃas, J., Papadopoulos, G. A., Polet, J., Romano, F., Salamon, A., Scala, A., Stepinac, M., Tappin, D. R., Thio, H. K., Tonini, R., Triantafyllou, I., Ulrich, T., Varini, E., Volpe, M., & Vyhmeister, E., 2021. Probabilistic tsunami hazard and risk analysis: A review of research gaps, *Frontiers in Earth Science*, **9**.

Berryman, K., Wallace, L., Hayes, G., Bird, P., Wang, K., Basili, R., Lay, T., Pagani, M., Stein, R., Sagiya, T., Rubin, C., Barreintos, S., Kreemer, C., Litchfield, N., Stirling, M., Gledhill, K., Haller, K., & Costa, C., 2015. The GEM Faulted Earth Subduction Interface Characterisation Project: Version 2.0 - April 2015, Tech. rep., GEM.

Bolker, B. M., 2008. *Ecological Models and Data in R*, Princeton University Press, Princeton, NJ.

Cheung, K. F., Lay, T., Sun, L., & Yamazaki, Y., 2022. Tsunami size variability with rupture depth, *Nature Geoscience*, **15**, 33–36.

Dall'Osso, F., Dominey-Howes, D., Moore, C., Summerhayes, S., & Withycombe, G., 2014. The exposure of Sydney (Australia) to earthquake-generated tsunamis, storms and sea level rise: a probabilistic multi-hazard approach, *Scientific Reports*, **4:7401**.

Davies, G., 2019. Tsunami variability from uncalibrated stochastic earthquake models: tests against deep ocean observations 2006-2016, *Geophysical Journal International*, **218**(3), 1939–1960.

Davies, G. & Griffin, J., 2018. The 2018 Australian Probabilistic Tsunami Hazard Assessment: Hazards from earthquake generated tsunamis., Tech. rep., Geoscience Australia Record 2018/41.

Davies, G. & Griffin, J., 2020. Sensitivity of Probabilistic Tsunami Hazard Assessment to Far-Field Earthquake Slip Complexity and Rigidity Depth-Dependence: Case Study of Australia, *Pure and Applied Geophysics*, **177**, 1521–1548.

Davies, G., Romano, F., & Lorito, S., 2020. Global Dissipation Models for Simulating Tsunamis at Far-Field Coasts up to 60 hours Post-Earthquake: Multi-Site Tests in Australia, *Frontiers in Earth Science*, **8**, 497.

Davies, G., Weber, R., Wilson, K., & Cummins, P., 2022. From offshore to onshore probabilistic tsunami hazard assessment via efficient Monte Carlo sampling, *Geophysical Journal International*, **230**(3), 1630–1651.

De Risi, R. & Goda, K., 2017. Simulation-based probabilistic tsunami hazard analysis: Empirical and robust hazard predictions, *Pure and Applied Geophysics*, **174**(8), 3083–3106.

Giblin, J., Damlamian, H., Davies, G., Weber, R., & Wilson, K., 2022. Earthquake Scenario Selection for Tsunami Inundation Hazard Assessment: Guidelines on using the 2018 Probabilistic Tsunami Hazard Assessment in the Pacific, Tech. rep., SPC and Geoscience Australia.

Grezio, A., Babeyko, A., Baptista, M. A., Behrens, J., Costa, A., Davies, G., Geist, E. L., Glimsdal, S., Gonzalez, F. I., Griffin, J., Harbitz, C. B., LeVeque, R. J., Lorito, S., Løvholt, F., Omira, R., Mueller, C., Paris, R., Parsons, T., Polet, J., Power, W., Selva, J., Sørensen, M. B., & Thio, H. K., 2017. Probabilistic tsunami hazard analysis: Multiple sources and global applications, *Reviews of Geophysics*, **55**(4), 1158–1198, 2017RG000579.

Helsel, D. & Hirsch, R., 2002. Statistical methods in water resources, *Techniques of Water-Resources Investigations of the United States Geological Survey, Book 4, Hydrologic Analysis and Interpretation*.

Kain, C., 2022. Technical Report on Tsunami Inundation Modelling for the East Coast of Tasmania, Tech. rep., Geological Survey Branch Mineral Resources Tasmania.

Lynett, P., Wei, Y., & Arcas, D., 2016. Tsunami hazard assessment: Best modeling practices and state-of-the-art technology, Tech. rep., Office of Nuclear Regulatory Research.

McCaffrey, R., 2009. The Tectonic Framework of the Sumatran Subduction Zone, *Annual Review of Earth and Planetary Sciences*, **37**, 345–366.

NTHMP, 2012. Proceedings and Results of the 2011 NTHMP Model Benchmarking Workshop, Tech. rep., National Tsunami Hazard Mitigation Program, NOAA Special Report.

NTHMP, 2017. Proceedings and Results of the National Tsunami Hazard Mitigation Program 2015 Tsunami Current Modeling Workshop, Tech. rep., National Tsunami Hazard Mitigation Program 2015.

Power, W., Wang, X., Wallace, L., Clark, K., & Mueller, C., 2017. The New Zealand Probabilistic Tsunami Hazard Model: development and implementation of a methodology for estimating tsunami hazard nationwide, *Geological Society, London, Special Publications*, **456**.

Tonini, R., Di Manna, P., Lorito, S., Selva, J., Volpe, M., Romano, F., Basili, R., Brizuela, B., Castro, M. J., de la Asuncion, M., Di Bucci, D., Dolce, M., Garcia, A., Gibbons, S. J., Glimsdal, S., Gonzalez-Vida, J. M., Løvholt, F., Macias, J., Piatanesi, A., Pizzimenti, L., Sanchez-Linares, C., & Vittori, E., 2021. Testing Tsunami Inundation Maps for Evacuation Planning in Italy, *Frontiers in Earth Science*, **9**.

Williamson, A. L., Rim, D., Adams, L. M., LeVeque, R. J., Melgar, D., & González, F. I., 2020. A source clustering approach for efficient inundation modeling and regional scale probabilistic tsunami hazard assessment, *Frontiers in Earth Science*, **8**.

Zamora, N., Catalan, P. A., Gubler, A., & Carvajal, M., 2021. Microzoning tsunami hazard by combining flow depths and arrival times, *Frontiers in Earth Science*, **8**.